UC San Diego
UC San Diego Previously Published Works

Title

Tissue mechanics govern the rapidly adapting and symmetrical response to touch

Permalink

Journal

ISSN

Authors

Eastwood, Amy L
Sanzeni, Alessandro
Petzold, Bryan C
et al.

Publication Date

DOI

Peer reviewed

Tissue mechanics govern the rapidly adapting and symmetrical response to touch

Amy L. Eastwood[a,1], Alessandro Sanzeni[b,c,1], Bryan C. Petzold[d,1], Sung-Jin Park[d,2], Massimo Vergassola[b], Beth L. Pruitt[d], and Miriam B. Goodman[a,3]

[a]Department of Molecular and Cellular Physiology, Stanford University School of Medicine, Stanford, CA 94305; [b]Department of Physics, University of California, San Diego, CA 92093; [c]Department of Physics and Istituto Nazionale di Fisica Nucleare (INFN), University of Milano, 20133 Milan, Italy; and [d]Department of Mechanical Engineering, Stanford University, Stanford, CA 94305

Interactions with the physical world are deeply rooted in our sense of touch and depend on ensembles of somatosensory neurons that invade and innervate the skin. Somatosensory neurons convert the mechanical energy delivered in each touch into excitatory membrane currents carried by mechanoelectrical transduction (MeT) channels. Pacinian corpuscles in mammals and touch receptor neurons (TRNs) in *Caenorhabditis elegans* nematodes are embedded in distinctive specialized accessory structures, have low thresholds for activation, and adapt rapidly to the application and removal of mechanical loads. Recently, many of the protein partners that form native MeT channels in these and other somatosensory neurons have been identified. However, the biophysical mechanism of symmetric responses to the onset and offset of mechanical stimulation has eluded understanding for decades. Moreover, it is not known whether applied force or the resulting indentation activate MeT channels. Here, we introduce a system for simultaneously recording membrane current, applied force, and the resulting indentation in living *C. elegans* (Feedback-controlled Application of mechanical Loads Combined with in vivo Neurophysiology, FALCON) and use it, together with modeling, to study these questions. We show that current amplitude increases with indentation, not force, and that fast stimuli evoke larger currents than slower stimuli producing the same or smaller indentation. A model linking body indentation to MeT channel activation through an embedded viscoelastic element reproduces the experimental findings, predicts that the TRNs function as a band-pass mechanical filter, and provides a general mechanism for symmetrical and rapidly adapting MeT channel activation relevant to somatosensory neurons across phyla and submodalities.

mechanosensitive ion channels | MEMS-based tools | mechanobiology | somatosensation | cellular electrophysiology

Our perception and reaction to the surrounding physical world is deeply rooted in our sense of touch. Pain sensation is palpably crucial for survival, and even the gentlest of touches is vital. For instance, lack of tactile sensory stimuli at the beginning of life has adverse effects on growth and neuronal development (1). Mammalian skin is invaded by a multitude of mechanoreceptor neurons that vary in their sensitivity to mechanical loads, their response dynamics, and their structure (2, 3). This diversification makes touch sensation robust, but it also complicates efforts to decipher its biophysical, genetic, and molecular basis. Whereas the recent analysis of the Piezo2 channel provides a critical entry point for future studies (4–7) of the molecules responsible for touch, little is currently understood about how external mechanical loads activate sensory mechanoelectrical transduction (MeT) channels in any animal. Even less is known about how skin transmits and filters mechanical energy. To investigate these questions, we exploited the experimental advantages of the nematode *Caenorhabditis elegans*, including the ability to obtain whole-cell patch-clamp recordings from identified mechanoreceptor neurons in living animals.

Adult *C. elegans* hermaphrodites are known to have five classes of mechanoreceptor neurons that exhibit surprisingly similar patterns of rapidly adapting and nearly symmetrical on and off MeT currents in response to applied mechanical loads

(reviewed in ref. 8). In four classes, including the touch receptor neurons (TRNs), such currents are sodium dependent and amiloride sensitive. Genetic dissection links these MeT currents to DEG/ENaC (degenerin/epithelial sodium channel) proteins in the TRNs (9–13) and a ciliated nociceptor (14–16). A transient receptor potential protein performs the role in a fifth class of mechanoreceptor that functions as a texture sensor (9, 17–20). Both kinds of ion channels also contribute to touch and pain sensation in *Drosophila* larvae (9, 11, 14, 21–25). Collectively, these observations suggest that no single class of proteins is responsible for forming sensory MeT channels and that the properties of rapid adaptation and symmetrical on and off responses are not uniquely linked to a single class of channel proteins.

The earliest insight into mechanisms of rapid adaptation emerged from work on the mammalian Pacinian corpuscle in the 1960s, which linked their rapid and symmetric responses to the onion-like lamellar capsule that encases its specialized nerve ending (9, 11–13, 19, 26–29). This multilayered accessory structure has been proposed to function as a purely mechanical filter (14, 17, 30) or as a mechanochemical filter embodied in a feedback loop in which GABAergic signals from the lamellar capsule are thought to suppress action potentials during a sustained stimulus (12, 13, 16, 18, 20, 25, 28). But, rapidly adapting MeT currents are found in other mammalian sensory afferents

Significance

Recordings from Pacinian corpuscles in the 1960s showed that touch elicits symmetric activation followed by rapid adaptation. Sinusoidal stimulation resulted in frequency doubling within a sensitive frequency band, suggesting that these receptors function as frequency-tuned vibration sensors. At the time, the surrounding lamellar capsule was proposed to generate these response dynamics by acting as a mechanical filter. However, similar response dynamics have since been seen in many other mechanoreceptors, leading to controversy over the specificity of this hypothesis. Using a combination of in vivo electrophysiology, feedback-controlled mechanical stimulation, and simulation, we resolve this controversy in favor of a systems-level mechanical filter that is independent of specific anatomical features or specific mechanoelectrical transduction channels.

such as those thought to innervate Meissner's corpuscles and hair follicles (reviewed in refs. 8, 31). Moreover, all of the mechanoreceptor neurons in *C. elegans* lack accessory structures analogous to the Pacinian corpuscle, yet they still exhibit rapid adaptation. Thus, rapidly adapting neural responses do not hinge on specialized accessory structures.

Rapid adaptation may be an autonomous and intrinsic property of MeT channels or a systems-level property that depends on the organization of such channels in their natural setting. Piezo2 is required for rapidly adapting touch-evoked currents in Merkel cells in whisker follicles (32–34) and results in rapidly adapting, mechanically activated channels when expressed in heterologous cells (35, 36), observations consistent with intrinsic or cell-autonomous mechanisms. Similarly and as noted above, channels dependent on the DEG/ENaC MeT protein MEC-4 rapidly activate and adapt to sustained mechanical loads in their native setting (12, 37). In contrast with Piezo2 channels, however, MEC-4–dependent channels are constitutively active (26, 38) when expressed in heterologous cells. This latter observation is consistent with the idea that mechanical activation and its response dynamics reflect not only the intrinsic mechanosensitivity of MeT channels, but also the systems-level mechanics and material properties of the innervated tissue.

We reasoned that efforts to differentiate between intrinsic and systems-level mechanisms would be accelerated by tools that could apply mechanical loads and measure their impact on tissue deformation and membrane current in parallel under conditions that maintained the integrity of the entire touch-sensing system. To this end we developed FALCON (Feedback-controlled Application of mechanical Loads Combined with in vivo Neurophysiology), a system that couples feedback-controlled mechanical stimulation with in vivo whole-cell patch-clamp recording. Force-feedback control is achieved by custom, force-sensing silicon microcantilevers with integrated piezoresistive strain gauges (39–41). This system can operate either in displacement clamp, delivering defined displacements while measuring applied force, or in force clamp, delivering defined forces while measuring applied displacement (32, 34, 42, 43). As we show here, the resulting data on applied mechanical force, body indentation, and evoked MeT currents enable detailed investigation of the physical parameters that govern activation of TRNs, as well as quantitative physical modeling.

Whether delivering force or displacement, systems for mechanical stimulation used by us and others to investigate MeT currents in *C. elegans* have lacked feedback control (12, 13, 16, 18, 20, 44). Similar open-loop systems are in widespread use for analysis of mammalian somatosensory neurons (45, 46) and cannot distinguish between changes in stimulus amplitude and channel adaptation, regardless of whether stimuli are reported as applied force or stimulator displacement. FALCON circumvents this limitation by combining closed-loop mechanical stimulation with in vivo whole-cell patch-clamp recording of membrane current (Fig. 1 and Fig. S1).

Here, we use this system to show that TRN MeT currents increase with body indentation, not applied force, and with stimulation rate, and we develop a mechanical model that reproduces the main dynamical features of MeT current activation in vivo.

Results

Mechanical Loads Evoke Rapidly Adapting "On" and "Off" MeT Currents Independent of Delivery Mode or Tissue Stiffness. We first asked how MeT current adaptation was affected by variations in the mechanics of the worm's body. To address this question, we prepared worms using two dissection procedures, a strategy enabling us to compare MeT currents in two distinct mechanical regimes. The first procedure was the standard slit-worm dissection procedure, which releases a portion of the gonad and intestines to reduce internal pressure and ease successful dissection of neuronal cell bodies (10, 47). The second was a more recently established dissection procedure that better preserves the physical integrity

Fig. 1. Rapid adaptation is independent of the stimulus delivery or dissection method. (*A*) The experimental preparation and integration with the FALCON system for simultaneous feedback-controlled mechanical stimulation and patch-clamp recording. A minimal dissection exposes only the anterior touch receptor neuron (ALM) cell body (*Left*), and the slit-worm preparation exposes the gonad, intestines, and ALM cell body (*Center*). A micrograph shows the position of the microcantilever with respect to the ALM cell body (*Right*). (*B*) Schematic drawing of a cross-section of the worm's body and position of the TRNs with respect to the cuticle, epidermis, and body wall muscle and the microcantilever. (*C*) The slit-worm preparation decreases body stiffness compared with the minimal dissection procedure (blue, *n* = 21 soft worms; red, *n* = 4 stiff worms). Curves show the relationship between force and indentation for individual worms. (*D–F*) Representative force (*F*), indentation (*z*), and membrane current (*I*) traces for recordings in a stiff worm evoked by a force-clamped single-step protocol (*D*) and in a soft worm evoked by a force-clamped (*E*) and displacement-clamped single-step protocol (*F*). The dashed lines illustrate the deconvolved fits of the indentation creep (*E*, $\tau = 34$ ms) and force relaxation (*F*, $\tau = 45$ ms) observed in soft worms during force-clamped and displacement-clamped recordings, respectively. Similar results were obtained in a total of 2 and 21 recordings from soft worms analyzed under displacement and force clamp, respectively, and 4 recordings from stiff worms analyzed under force clamp. Each trace is the average of between 10 and 14 trials.

of the nematode by exposing only the neuronal cell body of interest (48–50) (Fig. 1*A*). We applied mechanical loads by aligning the glass microsphere attached to the tip of the cantilever

with the top surface of the animal, which was its left side (Fig. 1 *A* and *B*). The slit-worm dissection procedure resulted in worms that are ~60–90% softer than those prepared with the less-invasive dissection procedure (Fig. 1*C*), which had an average effective stiffness of 1.1 ± 0.3 N/m (mean ± SD, $n = 4$). This value is similar to those measured previously for immobilized or freely moving intact animals (12, 42, 51, 52). For brevity, we refer to the worms prepared by the slit-worm procedure as "soft" and those prepared by the less-invasive dissection as "stiff."

Regardless of the dissection method and body stiffness (Fig. 1 *D* and *E*) or whether stimuli were delivered under force clamp or displacement clamp (Fig. 1 *E* and *F*), MeT currents adapt rapidly and activate in response to the application and withdrawal of mechanical loads. For instance, in recordings obtained from stiff and soft worms subjected to large force-clamped mechanical loads, the mean time constant for MeT current adaptation was 23 ms ($n = 2$, $F = 5$ μN) and 24 ± 11 ms (mean ± SD, $n = 21$, $F = 1$ μN), respectively. The average adaptation time constant of MeT currents evoked by large, displacement-clamped mechanical loads was 22 ms ($n = 2$, soft worms, $x_t = 5$ μm). These values are similar to those reported previously using open-loop mechanical stimulation methods (12, 13, 44, 53). Importantly, these adaptation rates are decoupled from the rate of stimulation because the closed-loop rise time was much faster than MeT current adaptation in all cases, varying from 4 ms ($n = 2$, stiff worms under force clamp, $F = 5$ μN) to 6 ± 2 ms (mean ± SD, $n = 19$, soft worms under force clamp, $F = 1$ μN) to 8 ms ($n = 2$, soft worms under displacement clamp, $x_t = 5$ μm). These observations show that rapid adaptation persists under closed-loop mechanical stimulation and when the underlying body mechanics are fundamentally altered by the dissection method.

The dynamics of body mechanics, however, were sensitive to the preparation method. In soft worms the indentation required to maintain constant force increased over time, a mechanical process known as creep (Fig. 1*E*, *Middle*). The average time constant for creep was 25 ± 11 ms (mean ± SD, $n = 21$ recordings from soft worms) at $F = 1$ μN, as estimated by deconvolution of the response with the stimulus profile (*Methods*). The force required to maintain constant indentation declined (force relaxation; Fig. 1*F*, *Top*) with an average time constant of 35 ms ($n = 2$ soft worms, $x_t = 5$ μm). However, indentation creep was not observed in recordings from stiff worms (Fig. 1*D*). Because MeT current adaptation rates were similar in both stiff and soft worms, the indentation creep and force relaxation that were only observed in soft worms cannot account for the rapid MeT current adaptation.

MeT Current Amplitude Depends on Indentation, Not Applied Force.
Having established procedures to analyze MeT currents under distinct mechanical regimes, we leveraged this manipulation to determine whether MeT current amplitude increased with applied force or the induced indentation. Conceptually, we rely on the fact that a given force is associated with a larger indentation in soft worms compared with stiff worms. As shown in Fig. 2, we found that the stiff mechanical regime shifts the midpoint of current-force *(I-F)* curves to higher forces ($F_{1/2} = 3.0$ μN and 0.38 μN for stiff and soft worms, respectively) and also significantly decreases sensitivity to force. (The slopes, δ_F, of the fitted *I-F* curves were 0.21 and 1.55 in soft and stiff worms, respectively.) In contrast, the midpoint and slope for current-indentation *(I-z)* curves were indistinguishable between the two mechanical regimes. (The midpoints, $z_{1/2}$, of the fitted functions were 2.4 μm and 2.9 μm in stiff and soft worms, respectively, and the slopes, δ_z, were 1.4 and 1.3 for soft and stiff worms, respectively.) Thus, MeT current amplitude increases in proportion to body indentation and not the applied force. This finding agrees with our recent study of behavioral sensitivity in *C. elegans* (42) and suggests that the probability of responding to

gentle touch follows MeT current amplitude. How might body indentation activate MeT channels? A simple model is that indentation induces strain and that it is this strain that serves as the proximal physical stimulus for activation of native MeT channels by external mechanical loads. Such a model predicts that MeT channels are sensitive to the velocity of the applied stimulus. Below, we test this model experimentally, as well as analytically through the development of a physical model.

MeT Currents Activate in Response to Fast, but Not Slow, Mechanical Stimuli.
We next asked how MeT channel activation was affected by varying the rate of mechanical stimulation. We delivered ramp-and-hold stimulus profiles in which a fixed indentation was delivered at variable rates and rapidly removed. The rapid offset provides a positive control for the presence of functional MeT channels whereas the variable onset rate tests the velocity sensitivity of MeT activation. We found that slow ramps failed to activate MeT currents, even though the steady-state indentation delivered in these experiments was sufficient to elicit robust off currents of similar amplitudes in all cases (Fig. 3*A*), suggesting that, unlike *Escherichia coli* MscS channels (54, 55), these channels do not silently inactivate in response to low-velocity stimulation. Thus, *C. elegans* TRNs and their MeT channels are sensitive to the velocity of stimulation.

Additionally, we determined the response to sinusoidal loading profiles that varied in frequency from 1 to 300 Hz and delivered forces that reached a peak-to-peak maximum of 1.96 ± 0.02 μN (mean ± SD, $n = 4$) at low frequencies, but declined in amplitude at high frequencies (Fig. 3*B*, *Top*). Consistent with the velocity dependence seen in response to ramp-and-hold stimuli, stimuli delivered at frequencies less than 3 Hz failed to elicit any detectable change in membrane current (Fig. 3*B*, *Bottom*). At 100 Hz, however, a significantly smaller peak-to-peak force of 0.45 ± 0.04 μN (mean ± SD, $n = 4$) produced a robust and sustained inward current. At intermediate frequencies and peak-to-peak amplitudes, MeT current exhibited oscillations with a significant power at twice the stimulus frequency (Fig. 3 *B* and *C*). Taken together, these results show that TRNs are vibration sensors insensitive to low (<3 Hz) frequency mechanical stimulation (Fig. 3*D*).

Biophysical Models of Symmetrical and Rapidly Adapting MeT Currents.
Having characterized how MeT currents respond to dynamic mechanical loads, we leveraged these experimental results to develop a mechanical model to further our understanding and to address questions about the physics of MeT channel activation. The general elements of the model are illustrated in Fig. 4 *A* and *B*, and the conceptual and mathematical formulation of the physical model is detailed in *Methods* and *SI Methods*. Heuristically, the application of mechanical loads to the skin is thought to generate time-dependent strain within the viscoelastic tissues that engulf the TRNs, and a hypothetical gating element links MeT channels to these viscoelastic tissues. For convenience we refer to the gating element as a filament and note that the role played by this filament could also be fulfilled by interactions between the MeT channel and the phospholipid bilayer. Differential displacements between MeT channels and their filaments result in an elongation of the filaments that is proportional to the velocity of indentation, and such elongation favors channel opening (*SI Methods*). Once the MeT channels open, the model asserts that elastic and viscous (friction) forces act to return the connected filaments to their relaxed conformation, closing the channels and accounting for rapid adaptation. This model offers an explanation for rapid adaptation, the symmetry between on and off responses (Figs. 1 *C–E* and 4 *C* and *D*), and the doubling of the frequency in the response to sinusoidal stimuli (Fig. 3 *B* and *C*).
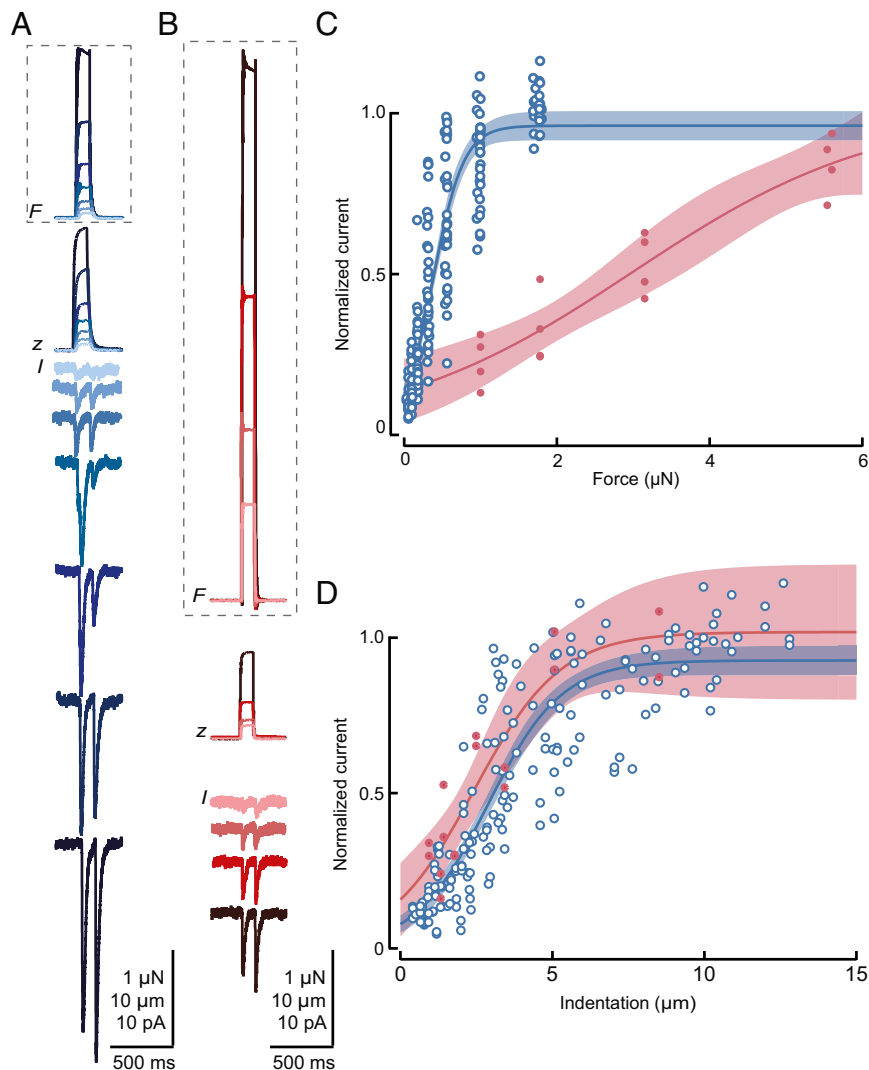
Fig. 2. MeT currents are sensitive to body indentation. (*A* and *B*) Force (*F*), indentation (*z*), and current (*I*) traces for recordings from a soft (blue traces) and stiff (red traces) worm, stimulated under force clamp between 0.05 and 6 µN. Similar results obtained in a total of 21 soft and 4 stiff worms. Each trace is the average of between 10 and 14 trials. (*C*) Peak current increases in proportion to force, but the apparent force dependence differs in soft ($n = 18$, blue) and stiff ($n = 2$, red) worms. (*D*) Peak current increases in proportion to indentation in both soft (blue) and stiff (red) worms. The data are from the same recordings as in *C*. Smooth lines in *C* and *D* are Boltzmann functions fit to the data; shaded area shows the 95% confidence interval for the fit. Fitting coefficients for force dependence in *C* are $F_{1/2}$, the force required for half-maximal activation, and δ_F, the slope of the curve, and have the following values: $F_{1/2} = 0.38$ µN and $\delta_F = 2.13$ for soft worms; $F_{1/2} = 3.0$ µN and $\delta_F = 1.55$ for stiff worms. Fitting coefficients for indentation in *D* are $z_{1/2}$, the indentation required for half-maximal activation, and δ_z, the slope of the curve, and have the following values: $z_{1/2} = 2.9$ µm and $\delta_z = 1.40$ for soft worms; $z_{1/2} = 2.4$ µm and $\delta_z = 1.25$ for stiff worms.

When the elastic and viscous forces are represented by the commonly used standard linear solid (SLS) model (9, 11), the model accurately predicts experimentally observed MeT currents evoked by pulse-like mechanical stimuli in soft worms (Fig. 4*C* and Fig. S2). Because the model also explicitly incorporates the relationship between mechanical loads and the average probability that MeT channels will be closed or enter subconductance and fully open states, it can also be used to predict the relationship between mechanical loads and channel states (Fig. 4*C*, *Middle*). The timescale and the profile of the predicted adapting current responses result from both the dynamic interplay of the MEC-4–dependent MeT channel's three main states—one closed, non-conducting state and two open, conducting states (14)—and the viscoelastic mechanical parameters of the model (see *Methods* and *SI Methods*). Whereas simulations included open and closed states, they did not include inactivated states because these were neither needed to account for MeT adaptation nor detected experimentally. Next, we challenged the model to reproduce the response generated by sinusoidal stimuli, and a common set of parameters was equally capable of predicting currents evoked by these more complicated mechanical loading profiles (Fig. 4*D*). We also asked whether or not the model could reproduce the response to arbitrary stimulus profiles, such as the one shown in Fig. 4*E*. The close agreement between the predicted response (black) and the experimental observations (green) underscores the robustness of the model.

A single set of optimized parameters (see Tables S1 and S2) reproduced the ensemble of data collected from each soft worm (Fig. 4 and Figs. S2 and S3), a finding that suggests that the properties that govern an individual worm's response to touch are fixed and independent of the type of mechanical stimulus applied. To further test this idea, we used the optimized parameters from the pulse-like mechanical stimuli to predict the sinusoidal, ramp-and-hold, and arbitrary stimuli, and we found a close agreement
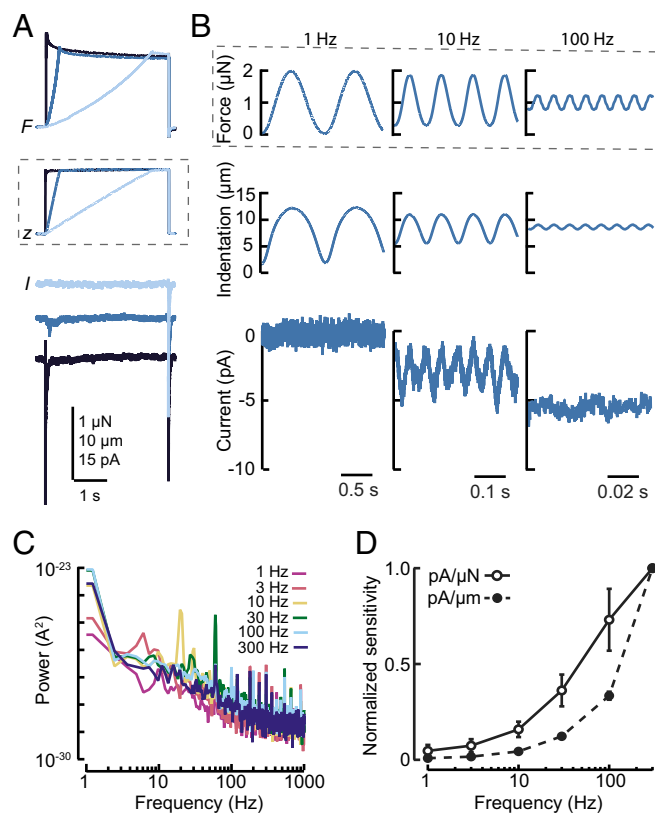
Fig. 3. *C. elegans* TRNs are sensitive to stimulus velocity and frequency. (*A*) Force (*F*), indentation (*z*), and current (*I*) recorded in a soft worm in response to ramp-and-hold stimuli delivered under displacement clamp (*n* = 1 worm). (*B*) Force, indentation, and current recording in a soft worm in response to sinusoidal stimuli delivered under force clamp. Similar results were obtained in a total of four recordings from soft worms. (*C*) Power spectra of currents elicited by sinusoidal stimuli applied to TRNs in a soft worm under force clamp. The prominent peaks at 6, 20, and 60 Hz correspond to stimulus frequencies of 3, 10, and 30 Hz, respectively, and illustrate that the TRNs generate nonlinear signals that are proportional to the structure of dynamic inputs. (*D*) Sensitivity of MeT currents as a function of stimulus frequency. Sensitivity is defined as the peak current amplitude divided by the applied force (peak-to-peak) or indentation achieved and has units of pA/μN (or pA/μm) before normalization to the value at the maximum frequency applied. Data were pooled from four recordings of soft worms stimulated under force clamp at the indicated frequencies.

between the predicted response and the experimental observations (Fig. S4). Further, when we predicted the theoretical response for one worm using the parameters optimized for another worm, we found a close overall agreement between the two (Fig. S3). Thus, there is a high degree of consistency between the optimal sets of model parameters across individual soft worms, despite variations in body stiffness that arise during the dissection procedure (Fig. 1C).

Our theoretical predictions are also robust with respect to certain details of the modeling. The so-called Kelvin model, the SLS model in the limit of vanishing memory of the friction force (9), already largely captures the MeT channel response (Figs. S5–S7). Furthermore, although three channel states (closed, fully open, and subconductance) were introduced to match the experimental observations of MEC-4–containing channels (14), MeT currents are already well reproduced by a simpler two-state model incorporating one closed and one open state (Figs. S6 and S7). In particular, the constitutive activity observed in Figs. 3B or 4D at high frequencies of sinusoidal stimulation is present in both models. Indeed, at high stimulus frequency the transitions

among the various conformational states no longer follow the input stimulus (Figs. S6 and S7), and the inertia of MeT channels makes the states populated by roughly constant fractions.

The bandwidth of FALCON was limited by the need to manually tune controller gains to optimally deliver a given stimulus and by the complexity of retuning during the course of a recording (*Methods*). This limitation prevented us from fully exploring the frequency response range of *C. elegans* TRNs and from experimentally testing whether the entire system behaves more like a high-pass or band-pass mechanical filter. Nevertheless, because the physical model closely fits the available experimental data (Figs. 4 and 5), we can use the model to speculate on the mechanical filter that shapes the response of *C. elegans* TRNs to time-varying, sinusoidal mechanical loads (i.e., vibration). General considerations on passive viscoelastic materials suggest that the force needed to generate a fixed-amplitude indentation of the cuticle should increase with frequency at high frequencies (9, 12, 13, 19, 26, 28). In this scenario the amplitude of the resulting indentations would be expected to decrease as their frequency increases. This decrease in indentation amplitude, in combination with the failure of slowly moving stimuli to activate currents, would produce a band-pass filter response. Fig. 5A shows the experimental results together with simulations based on this scenario. In simulations, but not experiments, we can also ask how the entire mechanical system operates under conditions in which the applied peak-to-peak force is independent of the stimulus frequency. As shown in Fig. 5B, this analysis reveals that indentation decreases with frequency and that the peak current and sensitivity of this preparation reach maximal values at 150 and 725 Hz, respectively. The simulation also reveals that current fluctuates at twice the input frequency and that the amplitude of such fluctuations declines with frequency (Fig. 5C). One model to explain this observation is that at high frequencies the channels dwell in open states and rarely visit the closed states. We note that these speculations about mechanical filtering in soft animals do not take into account variations in body stiffness among individuals or active mechanisms for modulating body stiffness during touch stimuli, which have been observed in other animals (e.g., ref. 30) and which would provide organism-level mechanisms for regulating the frequency dependence of touch sensation.

Discussion

The response dynamics presented here are shared by other rapidly adapting mechanosensory neurons, including *C. elegans* and *Drosophila* nociceptors (12, 13, 16, 18, 20, 25) and the neurons that innervate Pacinian and Meissner corpuscles and hair follicles in mammals (reviewed in refs. 31, 56). The fact that similar response dynamics are found across phyla and in sensory neurons that diverge radically in their morphology strongly suggests that this property arises from a common physical mechanism. Importantly, the model presented and validated here only requires a channel that responds and adapts to its environment through viscoelastic dynamics. Several molecular embodiments are compatible with our model, such as single or multiple elastic filaments tethered directly to the MeT channel or to a structure that occludes the ion permeation pathway that is pushed aside laterally by deformations of the skin. Furthermore, such filaments might be anchored to the extracellular matrix or to the cytoskeleton. Presently, experimental data make a direct linkage between the MeT channel and the microtubule cytoskeleton in TRNs unlikely (32, 34). However, such a connection has been proposed and characterized for campaniform sensilla in *Drosophila* adults and multidendritic nociceptors in larvae (35, 57). Finally, the viscoelastic dynamics we propose might arise from the plasma membrane itself, which suggests a proteinaceous tether to the MeT channel may not be a required element for gating under physiological conditions. Our model is compatible with this
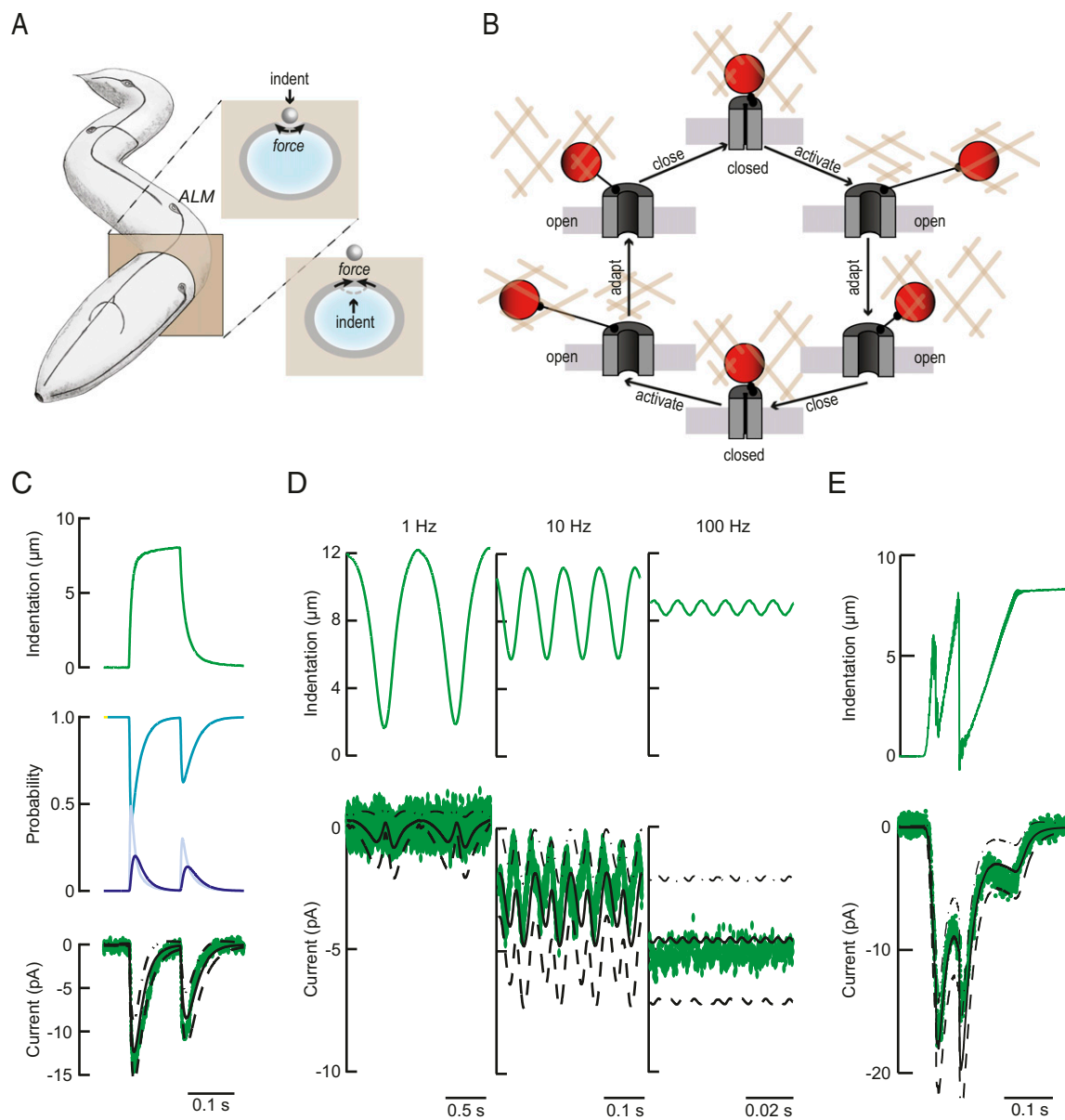
Eastwood et al.

Fig. 4. Reconstructing the response dynamics of MeT currents with a physical model of TRNs as viscoelastic mechanical filters. (*A*) Schematic showing forces orthogonal to the axis of indentation. (*B*) Schematic showing one possible embodiment of the model: an MeT channel linked through an elastic filament to an anchor (red ball) that can move through a viscous extracellular matrix. The system is at rest and the MeT channel is closed in the top and bottom panels. Moving from the top in a clockwise manner: internal forces generated from an external deformation induce a lateral shift between the extracellular matrix and anchor, stretching the filament and activating the channel; viscoelastic forces return the filament to its relaxed conformation, resulting in MeT channel adaptation and then closure; internal forces generated from releasing the external deformation induce a lateral shift in the extracellular matrix and anchor, stretching the filament and activating the channel; finally, viscoelastic forces conclude the cycle symmetrically. (*C*) Comparison of experimental and theoretical responses to a mechanical load applied under force clamp. Shown are (top to bottom) measured indentation, predicted MeT channel state probabilities as a function of time during stimulation, measured (green) and predicted macroscopic MeT currents (black). The SLS model parameters are described in the third row of Table S1. (*D*) Ensemble of measured (green) and predicted (black) MeT currents evoked by sinusoidal epochs sampled from recordings in a soft worm. Model parameters as in C. (*E*) MeT currents evoked by an arbitrary stimulus profile (green) and the response predicted using the same model parameters as in C and D (black).

"force-from-lipid" model (37). Identifying the microscopic and molecular nature of the mechanical unit will require targeted experiments to identify the viscoelastic elements and determine how such elements interact with MeT channels in situ. The findings and methods reported here provide the tools to manipulate key proteins and observe their effects on mechanics and adaptation.

The mechanism that we propose establishes an unexpected connection between two different mechanical senses: touch and

hearing. The elastic filament system is reminiscent of similar models originally proposed for hair cells (26), although with one major difference. Fast-adapting afferents respond symmetrically to touch, at both the onset and offset of a stimulus (Figs. 1 *C–E* and 4*C*). Conversely, the response of hair cells is asymmetric with respect to the application of force, e.g., responses are only seen at the onset of stimulations pointing toward the kinocilium of the hair bundle. The asymmetry is due to the controlled geometry of the tip links and less pronounced in immature hair
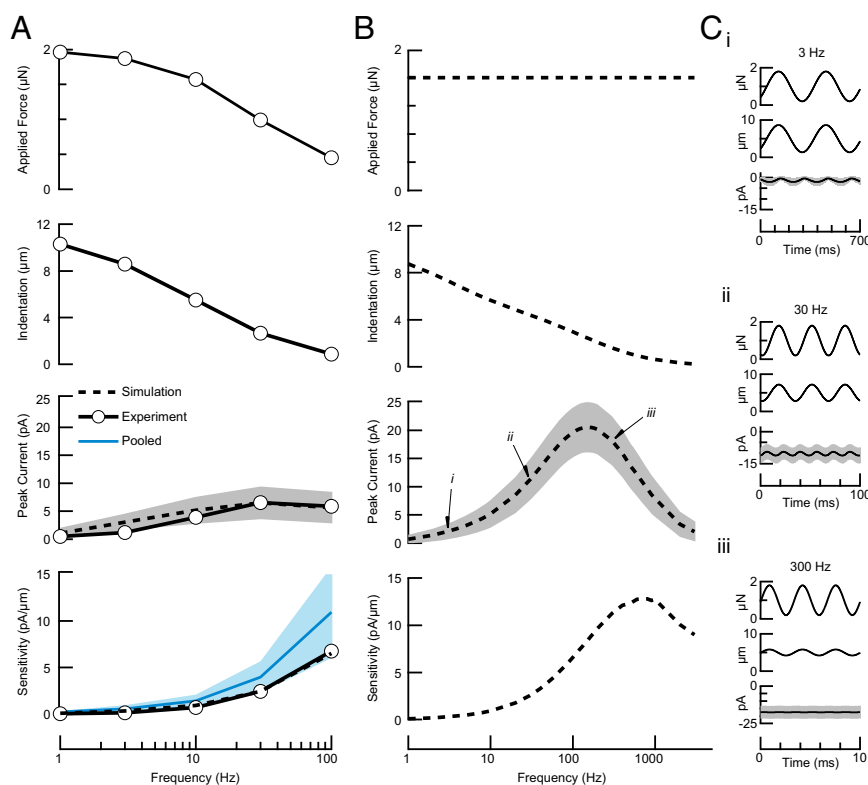
Fig. 5. Experimental and computational study of the frequency response of tactile sensation in soft animals. (*A*) Simulations using parameters optimized to fit responses to mechanical stimuli (Fig. 4) reproduce experimental responses to sinusoidal stimuli in a representative recording from a soft worm. Table S1 (third row) lists the parameters for the SLS model. Shown are (top to bottom) applied force (peak-to-peak), resulting indentation (peak-to-peak), peak current, and sensitivity (pA/μm). Solid black lines show experimental results from a representative recording; solid blue lines show results pooled across four recordings; dashed black lines show simulations; and shaded areas indicate the errors in measurement and simulation. Applied force declines with frequency due to limitations in the FALCON device. (*B*) Simulation of the mechanical and physiological response to applied force up to 3 kHz. Model parameters as in *A*. Shown are (top to bottom) applied force (peak), resulting indentation (peak), peak current, and sensitivity (pA/μm). Indentation declines with frequency as a result of the properties of the mechanical system, despite a constant amplitude of applied force. (*C*) Simulations of the indentation and currents evoked by sinusoidal force stimuli. Model parameters as in *A* and *B*. As found experimentally, the current varies at approximately twice the frequency of the stimulus, except at high frequencies where large current fluctuations decline.

cells when multiple tip links are present and their directions are still randomly oriented (39). The symmetry observed in *C. elegans* TRNs is predicted to arise from the mechanics of indentation through a thin cuticle and the ensuing strain in the filaments that occurs at both the onset and offset of stimulation in opposite directions yet with comparable amplitudes. However, whether symmetry holds at the level of individual MeT channels or whether it is only retained at the level of the whole mechanoreceptor neuron remains an open question. For the schema shown in Fig. 4, individual MeT channels would show symmetric on–off responses if, for instance, the attachment of the filament to the channel could slide along the circumference of the channel. This system would then be essentially analogous to a trapdoor occluding the channel and sliding laterally under mechanical stimulation. Conversely, if the point of attachment of the filaments were fixed, individual MeT channels would have a preference in their direction of stimulation, and on–off symmetry would be a macroscopic property of the whole neuron due to the random position of the channels and their putative filaments along the neurite (32, 34). Thus, in the absence of symmetry-breaking structures such as those found in vertebrate hair cells, insect bristles, or mammalian guard hairs (28, 58), we expect that systems characterized by somatosensory neurons embedded within thin tissues will generally feature on–off symmetry in their touch responses.

How might *C. elegans* use sensitivity to strain, velocity, and vibration? It has long been known that *C. elegans* TRNs are involved in sensing both gentle touch to the body and nonlocalized mechanical taps (reviewed in ref. 45). Worms reverse in response to anterior touch, an avoidance behavior that allows them to escape from predatory fungi (47). Our results suggest that a robust response from *C. elegans* TRNs requires a brief contact of sufficient indentation depth. This temporal and spatial threshold may ensure that TRNs do not interpret small particles like bacteria as aversive and back away from a potential food source. Filtering low frequencies may also enable TRNs to ignore body movements, which involve undulation frequencies on the order of 0.5 Hz when crawling on standard growth plates in the absence of food (e.g., refs. 48, 50). Thus, the fine-tuning of the system may help TRNs focus on responding to aversive mechanical stimuli, while leaving stimuli such as those produced by substrate texture and self-movement to other mechanoreceptor neurons.

Methods

Nematode Strains and Culture. Age-synchronized *C. elegans* nematodes were grown on standard OP50 growth plates at 20–22 °C. Wild-type worms were TU2769 [P*mec-17(uIs31) III*], an integrated strain that uses the *mec-17* promoter to express GFP exclusively in the TRNs that run along the body of the nematode, as previously described (12).

Electrophysiology. Worms were immobilized on thin agarose (2% wt/vol in extracellular saline) pads using WormGlu (GluStitch). Observations were made on a Nikon Eclipse FN1 microscope equipped with Nomarski-DIC optics, 60×/1.0 N.A. water immersion objective and a black and white CCD camera (JAI CV-A55IR C). In the majority of experiments, a large portion of the

gonad and intestines posterior to the vulva was dissected to release internal pressure, as previously described (10). In several of the experiments, the gonad and intestine were left in situ, as described in ref. 49. In all experiments a small incision was made immediately anterior to the cell body of the anterior touch receptor neuron, ALM.

All dissections were done using a sharp glass dissection tool mounted on a hydraulic manipulator (Narishige MMO-203). The cell body and posterior neurite of ALM remained intact and in place, as verified by viewing GFP fluorescence. Pharyngeal pumping and head movement were used to determine that worms were alive during recording. All recordings were from the ALM neuron on the left-hand side of the body with the stimulating cantilever placed just posterior to the pharynx bulb, ~150 μm away from the cell body (Fig. 1A). Other touch receptor neurons were inaccessible because of geometrical constraints imposed by the position of the stimulating cantilever and patch-clamp recording headstage.

Recording pipettes were pulled from borosilicate glass to a tip diameter of 2–4 mm on a P-97 micropipette puller (Sutter Instruments) and shaped by pressure polishing (59, 60). Pipettes had resistances of 6–17 MΩ when filled with normal internal saline (see below) and 20 mM sulforhodamine 101 (Invitrogen).

Membrane current and voltage were amplified and acquired with an EPC-10 amplifier and Patchmaster software (HEKA Instruments/Harvard Biosciences). Analog data were digitized at 10 kHz and filtered at 2.9 kHz. Whole-cell recordings were achieved by a combination of suction and a brief voltage pulse ("zap"), where success was verified by monitoring diffusion of GFP into the pipette and sulforhodamine-101 into the cell body.

External saline was composed of (in mM): NaCl (145), KCl (5), MgCl$_2$ (5), CaCl$_2$ (1), and Hepes (10), pH adjusted to 7.2 with KOH. The osmolarity of all external solutions was adjusted to ~325 mOsm with 20 mM D-glucose. Internal saline was composed of (in mM): K-gluconate (125), KCl (18), NaCl (4), MgCl$_2$ (1), CaCl$_2$ (0.6), Hepes (1), and EGTA (10), pH adjusted to 7.2 with KOH. The osmolarity of intracellular solutions was ~315 mOsm. All chemicals were purchased from Sigma.

FALCON. The FALCON system combines patch-clamp electrophysiology with a force-clamp system. The force-clamp system is similar to systems used previously to characterize body mechanics and behavioral responses to touch (5–7, 33, 36, 42, 43, 51, 52). It enables feedback-controlled delivery of user-defined forces (or displacements) and consists of a piezoresistive silicon cantilever, a piezoelectric actuator with a built-in strain gauge displacement sensor (P-841.10, Physik Instrumente), and a real-time controller (National Instruments, Compact Rio Field-programmable Gate Array). The cantilevers (30 μm wide, 750 μm long, 7 μm thick) were microfabricated, as previously reported (8, 12, 40, 41, 43). The piezoresistor serves as an integrated strain gauge to measure cantilever deflection; deflection is converted to force based on the calibrated cantilever spring constant, k_c. Cantilevers were bonded to printed circuit boards (5 mm wide, 29 mm long, 0.8 mm thick) with epoxy (Devcon) and connected to the measurement circuit through aluminum wirebonds. Five cantilevers were used over the course of these experiments, which had k_c values between 0.773 and 0.868 N/m and resonant frequencies in air between 15.2 and 16.2 kHz (Fig. S1B). Glass microspheres (10 ± 1-μm diameter borosilicate glass, ThermoFisher Scientific) were adhered to cantilever tips with a photocurable acrylic glue (Loctite 352, Henkel) to create a defined contact surface. Finally, aluminum wirebonds were covered with epoxy (Devcon), and then 600 nm of Parylene N (Specialty Coating Systems) was deposited on each device. This last step protects electrical components from exposure to saline during experiments. The printed circuit board was made with FR4 (Young's modulus = 11 GPa) and designed to be orders of magnitude stiffer than the cantilevers (k_{PCB} = 300 N/m). The measurement circuit consisted of the cantilever piezoresistor connected in a Wheatstone bridge configuration with two potentiometers and a temperature compensation resistor. The bridge bias was set at 2 V, and its output was amplified 1,000 times with an instrumentation amplifier (INA103).

Piezoresistive cantilevers were mounted to the piezoelectric actuator at a 10° angle. Because the device was placed directly above the worm's surface before each experiment, sample indentation depth (z) was calculated as $z = x_t − x_c$, where x_t is the total actuator displacement as measured by the built-in sensor on the actuator and x_c is the cantilever deflection as measured by the piezoresistor.

The real-time controller calculated and adjusted the driving voltage of the piezoelectric actuator to correct the error between the voltage signal from the piezoresistive cantilever and a desired setpoint. Feedback was delivered through a control loop operating at 100 kHz. The controller was connected to the EPC-10 amplifier through the CompactRio digital input system and triggered by a digital signal from the Patchmaster software (Harvard Bioscience) with a delay time of less than 2 μs. This circuitry ensured the control system produced the appropriate actuator command voltage for the desired actuator travel distance

and applied force. The system was calibrated by indenting a glass slide and verifying output voltage. Before each experiment the probe was positioned just out of contact with the worm, the Wheatstone bridge was balanced, and the feedback gain was manually adjusted to achieve the fastest rise time with minimal overshoot for the stimulus at the start of a stimulation protocol.

Data Analysis. Whole-cell capacitance and series resistance were measured as previously described (10, 12, 13, 38). Series resistance was not compensated, and membrane voltage was corrected for liquid junction potentials but not for errors resulting from uncompensated series resistance. Data analysis was performed with Igor Pro (Wavemetrics) and MATLAB (MathWorks).

Because of jitter in the timing of the delivery of mechanical stimulus pulses, it was necessary to align replicates post hoc and before averaging responses to stimulus presentations. The alignment was accomplished by maximizing the cross-correlation between small regions within one replicate and the identical regions within each of the other replicates (6–14 replicates total in a typical series). Once properly aligned, the force, displacement, and membrane current data were averaged.

To estimate the time constants for MeT channel activation and decay, we fit averaged current waveforms to the function

$$I(t) = G_{max} * (\exp(-t/\tau_2) - \exp(-t/\tau_1)) * (V_h - E_{Na}) + I_o,$$

where G_{max} is the estimated maximal conductance, V_h is the holding potential, E_{Na} is the Nernst potential for Na$^+$ ions in our solutions, I_o is the baseline current, and τ_1 and τ_2 are the activation and adaptation time constants, respectively. The decay of applied force observed under displacement clamp was fit with a single exponential. The indentation rise, or creep, observed when soft worms were stimulated under force clamp was fit with a double exponential, where the first time constant represented the rate of stimulus application and the second time constant represented the rate of creep. Rates were averaged for a single, large stimulus (1 μN for force-clamped soft worms, 5 μm for displacement-clamped soft worms, and 5 μN for force-clamped stiff worms).

To determine how current depends on applied force and indentation, peak current was plotted as a function of either force or indentation and the resulting curves were fit with the Boltzmann function

$$f(x) = I_{max} / (1 + \exp((X_{50} - x)/\delta)),$$

where I_{max} is the estimated maximal membrane current, X_{50} is the estimated half-maximal force or indentation, and δ is the slope that controls the steepness of the curve. The data were then normalized to the predicted I_{max} and pooled across recordings obtained under similar conditions with respect to dissection procedure (stiff, soft).

To estimate the rate of indentation creep in soft worms, we deconvolved the indentation time course with the applied force time course. To fit the range of indentations produced for 1 μN of force, we introduced a non-linearity that increases with indentation (15, 16, 40, 41). Similarly, to estimate the rate of force relaxation in soft worms, we deconvolved the force time course with the applied indentation time course.

Mean values are reported as mean ± SD throughout. Statistical analyses performed using IgorPro (Wavemetrics).

Modeling Activation of MeT Channels. Here, we describe the physical ingredients of the model developed to analyze and predict the response of *C. elegans* TRNs; the mathematical formulation of the model is detailed in *SI Methods*. We posited that each MeT channel in the plasma membrane of a TRN is linked to mechanical units (referred to as "anchors" for simplicity) via elastic filaments (Fig. 4B). In Fig. 4B, the filament and anchor are embedded in the extracellular matrix, but similar results would be obtained if these elements were embedded elsewhere. When the surface of the nematode is deformed, strain is produced in the cuticle (Fig. 4A) and we expect such strain to induce differential displacements between the channels and their anchors. The thinness of the cuticle (compared with its lateral extension) dictates that strain resulting from indentation orthogonal to the surface of the worm is strongest in the tangential plane (17–20, 42, 43). The result is that elastic filaments are elongated in opposite directions, but with roughly symmetrical amplitudes at the onset and the offset of a stimulus on the surface of the nematode (Fig. 4 A and B). Two additional forces determine the dynamics of the filament/anchor systems:(i) the Hookean force resulting from the elongation of the elastic filament, which tends to restore the relaxation distance of the filament; and (ii) friction forces between the extracellular matrix and the filament/anchor system, which resist their relative motion. We represented the combination of elastic and friction forces with models commonly used for viscoelastic materials (9, 11–13, 16, 18, 20–25, 44). In particular, the Kelvin and the SLS models yield the equations and

the results presented in the main text and in *SI Methods*. The Kelvin model contains a spring in parallel with a dashpot, whereas the SLS model contains a spring in parallel with a Maxwell module, which is itself another spring in series with a dashpot (9, 11, 27, 29, 46).

Further, we conjectured that activation of the MeT channels follows a Boltzmann function of the elongation of their linked filaments. Previous experimental observations showed that MEC-4–containing MeT channels adopt multiple open and closed states, including a prominent subconductance state (10, 14, 17). Therefore, we assumed that the channels transition between their closed and open states via a third conformation with intermediate conductance and that the transition rates among those conformational states respect detailed balance. As detailed in *SI Methods*, the

assumptions permit the use of experimental indentation profiles as inputs to derive predicted MeT currents. We then compared experimental curves to fit the parameters of our model and derived the results presented here.

1. Ardiel EL, Rankin CH (2010) The importance of touch in development. *Paediatr Child Health* 15(3):153–156.
2. Abraira VE, Ginty DD (2013) The sensory neurons of touch-. *Neuron* 79(4):618–639.
3. Lumpkin EA, Marshall KL, Nelson AM (2010) The cell biology of touch. *J Cell Biol* 191(2):237–248.
4. Ikeda R, Gu JG (2014) Piezo2 channel conductance and localization domains in Merkel cells of rat whisker hair follicles. *Neurosci Lett* 583:210–215.
5. Maksimovic S, et al. (2014) Epidermal Merkel cells are mechanosensory cells that tune mammalian touch receptors. *Nature* 509(7502):617–621.
6. Woo S-H, et al. (2014) Piezo2 is required for Merkel-cell mechanotransduction. *Nature* 509(7502):622–626.
7. Ranade SS, et al. (2014) Piezo2 is the major transducer of mechanical forces for touch sensation in mice. *Nature* 516(7529):121–125.
8. Geffeney SL, Goodman MB (2012) How we feel: Ion channel partnerships that detect mechanical inputs and give rise to touch and pain perception. *Neuron* 74(4):609–619.
9. Gutierrez-Lemini D (2014) *Engineering Viscoelasticity* (Springer, New York).
10. Goodman MB, et al. (1998) Active currents regulate sensitivity and dynamic range in C. elegans neurons. *Neuron* 20(4):763–772.
11. Christensen R (1982) *Theory of Viscoelasticity* (Academic, New York), 2nd Ed.
12. O'Hagan R, Chalfie M, Goodman MB (2005) The MEC-4 DEG/ENaC channel of Caenorhabditis elegans touch receptor neurons transduces mechanical signals. *Nat Neurosci* 8(1):43–50.
13. Arnadóttir J, O'Hagan R, Chen Y, Goodman MB, Chalfie M (2011) The DEG/ENaC protein MEC-10 regulates the transduction channel complex in Caenorhabditis elegans touch receptor neurons. *J Neurosci* 31(35):12695–12704.
14. Brown AL, Liao Z, Goodman MB (2008) MEC-2 and MEC-6 in the Caenorhabditis elegans sensory mechanotransduction complex: Auxiliary subunits that enable channel activity. *J Gen Physiol* 131(6):605–616.
15. Dayan P, Abbott LF (2001) *Theoretical Neuroscience: Computational and Mathematical Modeling of Neural Systems* (The MIT Press, Cambridge, MA).
16. Geffeney SL, et al. (2011) DEG/ENaC but not TRP channels are the major mechanoelectrical transduction channels in a C. elegans nociceptor. *Neuron* 71(5):845–857.
17. Loewenstein WR, Skalak R (1966) Mechanical transmission in a Pacinian corpuscle. An analysis and a theory. *J Physiol* 182(2):346–378.
18. Li W, Kang L, Piggott BJ, Feng Z, Xu XZS (2011) The neural circuits and sensory channels mediating harsh touch sensation in Caenorhabditis elegans. *Nat Commun* 2:315–319.
19. Landau LD, Lifshitz EM (1986) *Theory of Elasticity*, eds Landau LD, Lifshitz EM (Pergamon, Oxford), 3rd Ed.
20. Kang L, Gao J, Schafer WR, Xie Z, Xu XZS (2010) C. elegans TRP family protein TRP-4 is a pore-forming subunit of a native mechanotransduction channel. *Neuron* 67(3):381–391.
21. Cheng LE, Song W, Looger LL, Jan LY, Jan YN (2010) The role of the TRP channel NompC in Drosophila larval and adult locomotion. *Neuron* 67(3):373–380.
22. Gorczyca DA, et al. (2014) Identification of Ppk26, a DEG/ENaC Channel functioning with Ppk1 in a mutually dependent manner to guide locomotion behavior in Drosophila. *Cell Reports* 9(4):1446–1458.
23. Mauthner SE, et al. (2014) Balboa binds to pickpocket in vivo and is required for mechanical nociception in Drosophila larvae. *Curr Biol* 24(24):2920–2925.
24. Zhong L, Hwang RY, Tracey WD (2010) Pickpocket is a DEG/ENaC protein required for mechanical nociception in Drosophila larvae. *Curr Biol* 20(5):429–434.
25. Yan Z, et al. (2013) Drosophila NOMPC is a mechanotransduction channel subunit for gentle-touch sensation. *Nature* 493(7431):221–225.
26. Howard J, Hudspeth AJ (1988) Compliance of the hair bundle associated with gating of mechanoelectrical transduction channels in the bullfrog's saccular hair cell. *Neuron* 1(3):189–199.
27. Mendelson M, Lowenstein WR (1964) Mechanisms of receptor adaptation. *Science* 144(3618):554–555.
28. Pawson L, et al. (2009) GABAergic/glutamatergic-glial/neuronal interaction contributes to rapid adaptation in pacinian corpuscles. *J Neurosci* 29(9):2695–2705.
29. Loewenstein WR, Mendelson M (1965) Components of receptor adaptation in a Pacinian corpuscle. *J Physiol* 177:377–397.
30. Tytell ED, Hsu C-Y, Williams TL, Cohen AH, Fauci LJ (2010) Interactions between internal forces, body stiffness, and fluid environment in a neuromechanical model of lamprey swimming. *Proc Natl Acad Sci USA* 107(46):19832–19837.
31. Zimmerman A, Bai L, Ginty DD (2014) The gentle touch receptors of mammalian skin. *Science* 346(6212):950–954.
32. Cueva JG, Mulholland A, Goodman MB (2007) Nanoscale organization of the MEC-4 DEG/ENaC sensory mechanotransduction channel in Caenorhabditis elegans touch receptor neurons. *J Neurosci* 27(51):14089–14098.
33. Ikeda R, et al. (2014) Merkel cells transduce and encode tactile stimuli to drive Aβ-afferent impulses. *Cell* 157(3):664–675.
34. Emtage L, Gu G, Hartwieg E, Chalfie M (2004) Extracellular proteins organize the mechanosensory channel complex in C. elegans touch receptor neurons. *Neuron* 44(5):795–807.
35. Liang X, et al. (2013) A NOMPC-dependent membrane-microtubule connector is a candidate for the gating spring in fly mechanoreceptors. *Curr Biol* 23(9):755–763.
36. Coste B, et al. (2010) Piezo1 and Piezo2 are essential components of distinct mechanically activated cation channels. *Science* 330(6000):55–60.
37. Anishkin A, Loukin SH, Teng J, Kung C (2014) Feeling the hidden mechanical forces in lipid bilayer is an original sense. *Proc Natl Acad Sci USA* 111(22):7898–7905.
38. Goodman MB, et al. (2002) MEC-2 regulates C. elegans DEG/ENaC channels needed for mechanosensation. *Nature* 415(6875):1039–1042.
39. Waguespack J, Salles FT, Kachar B, Ricci AJ (2007) Stepwise morphological and functional maturation of mechanotransduction in rat outer hair cells. *J Neurosci* 27(50):13890–13902.
40. Doll JC, Park S-J, Pruitt BL (2009) Design optimization of piezoresistive cantilevers for force sensing in air and water. *J Appl Phys* 106(6):64310.
41. Park SJ, Doll JC, Pruitt BL (2010) Piezoresistive cantilever performance-Part I: Analytical model for sensitivity. *J Microelectromech Syst* 19(1):137–148.
42. Petzold BC, Park S-J, Mazzochette EA, Goodman MB, Pruitt BL (2013) MEMS-based force-clamp analysis of the role of body stiffness in C. elegans touch sensation. *Integr Biol (Camb)* 5(6):853–864.
43. Park S-J, Petzold BC, Goodman MB, Pruitt BL (2011) Piezoresistive cantilever force-clamp system. *Rev Sci Instrum* 82(4):043703.
44. Chen X, Chalfie M (2015) Regulation of mechanosensation in C. elegans through ubiquitination of the MEC-4 mechanotransduction channel. *J Neurosci* 35(5):2200–2212.
45. Chalfie M (2009) Neurosensory mechanotransduction. *Nat Rev Mol Cell Biol* 10(1):44–52.
46. Hao J, Delmas P (2011) Recording of mechanosensitive currents using piezoelectrically driven mechanostimulator. *Nat Protoc* 6(7):979–990.
47. Maguire SM, Clark CM, Nunnari J, Pirri JK, Alkema MJ (2011) The C. elegans touch response facilitates escape from predacious fungi. *Curr Biol* 21(15):1326–1330.
48. Cronin CJ, et al. (2005) An automated system for measuring parameters of nematode sinusoidal movement. *BMC Genet* 6:5.
49. Lindsay TH, Thiele TR, Lockery SR (2011) Optogenetic analysis of synaptic transmission in the central nervous system of the nematode Caenorhabditis elegans. *Nat Commun* 2:306–309.
50. Fang-Yen C, et al. (2010) Biomechanical analysis of gait adaptation in the nematode Caenorhabditis elegans. *Proc Natl Acad Sci USA* 107(47):20323–20328.
51. Park S-J, Goodman MB, Pruitt BL (2007) Analysis of nematode mechanics by piezoresistive displacement clamp. *Proc Natl Acad Sci USA* 104(44):17376–17381.
52. Petzold BC, et al. (2011) Caenorhabditis elegans body mechanics are regulated by body wall muscle tone. *Biophys J* 100(8):1977–1985.
53. Bounoutas A, O'Hagan R, Chalfie M (2009) The multipurpose 15-protofilament microtubules in C. elegans have specific roles in mechanosensation. *Curr Biol* 19(16):1362–1367.
54. Akitake B, Anishkin A, Sukharev S (2005) The "dashpot" mechanism of stretch-dependent gating in MscS. *J Gen Physiol* 125(2):143–154.
55. Belyy V, Anishkin A, Kamaraju K, Liu N, Sukharev S (2010) The tension-transmitting 'clutch' in the mechanosensitive channel MscS. *Nat Struct Mol Biol* 17(4):451–458.
56. Delmas P, Hao J, Rodat-Despoix L (2011) Molecular mechanisms of mechanotransduction in mammalian sensory neurons. *Nat Rev Neurosci* 12(3):139–153.
57. Zhang W, et al. (2015) Ankyrin repeats convey force to gate the NOMPC mechanotransduction channel. *Cell* 162(6):1391–1403.
58. Katta S, Krieg M, Goodman MB (2015) Feeling force: cells and molecules enabling sensory mechanotransduction. *Ann Rev Cell Dev Biol* 31:347–371.
59. Goodman MB, Lockery SR (2000) Pressure polishing: A method for re-shaping patch pipettes during fire polishing. *J Neurosci Methods* 100(1-2):13–15.
60. Johnson BE, Brown AL, Goodman MB (2008) Pressure-polishing pipettes for improved patch-clamp recording. *J Vis Exp* (20):e964.
61. Ventsel E, Krauthammer T (2001) *Thin Plates and Shells* (Marcel Dekker, Basel).
62. Phillips RB, Kondev J, Theriot J (2009) *Physical Biology of the Cell* (Garland Science, New York).
63. Vella D, Ajdari A, Vaziri A, Boudaoud A (2012) The indentation of pressurized elastic shells: From polymeric capsules to yeast cells. *J R Soc Interface* 9(68):448–455.

Eastwood et al.